New Journal of Physics
The open access journal at the forefront of physics

Deutsche Physikalische Gesellschaft DPG IOP Institute of Physics

PAPER • OPEN ACCESS

Complete phase retrieval of photoelectron wavepackets

To cite this article: L Pedrelli *et al* 2020 *New J. Phys.* **22** 053028

New Journal of Physics
The open access journal at the forefront of physics

Deutsche Physikalische Gesellschaft DPG
IOP Institute of Physics

Published in partnership with: Deutsche Physikalische Gesellschaft and the Institute of Physics

OPEN ACCESS

RECEIVED
16 December 2019

REVISED
25 March 2020

ACCEPTED FOR PUBLICATION
26 March 2020

PUBLISHED
19 May 2020

PAPER

Complete phase retrieval of photoelectron wavepackets

L Pedrelli[1,4], P D Keathley[2,4], L Cattaneo[1], F X Kärtner[2,3] and U Keller[1]

[1] Physics Department, Institute of Quantum Electronics, ETH Zürich, 8093 Zürich, Switzerland
[2] Research Laboratory of Electronics, Massachusetts Institute of Technology, Cambridge, MA 02139, United States of America
[3] Center of Free-Electron Laser Science, DESY and Department of Physics, University of Hamburg, D-22607 Hamburg, Germany
[4] L Pedrelli and P D Keathley contributed equally to this work.

E-mail: lucaped@phys.ethz.ch

Keywords: attosecond science, strong-field physics, atomic, optical and molecular physics, ultrafast science

Supplementary material for this article is available online

Abstract

Coherent, broadband pulses of extreme ultraviolet light provide a new and exciting tool for exploring attosecond electron dynamics. Using photoelectron streaking, interferometric spectrograms can be generated that contain a wealth of information about the phase properties of the photoionization process. If properly retrieved, this phase information reveals attosecond dynamics during photoelectron emission such as multielectron dynamics and resonance processes. However, until now, the full retrieval of the continuous electron wavepacket phase from isolated attosecond pulses has remained challenging. Here, after elucidating key approximations and limitations that hinder one from extracting the coherent electron wavepacket dynamics using available retrieval algorithms, we present a new method called absolute complex dipole transition matrix element reconstruction (ACDC). We apply the ACDC method to experimental spectrograms to resolve the phase and group delay difference between photoelectrons emitted from Ne and Ar. Our results reveal subtle dynamics in this group delay difference of photoelectrons emitted form Ar. These group delay dynamics were not resolvable with prior methods that were only able to extract phase information at discrete energy levels, emphasizing the importance of a complete and continuous phase retrieval technique such as ACDC. Here we also make this new ACDC retrieval algorithm available with appropriate citation in return.

1. Introduction

When high-energy photons interact with a gas target, photoelectrons are generated. While the rate of this photoelectron generation can be described by the gas species' cross-section, the attosecond dynamics of the emission process are more difficult to resolve [1–3]. Revealing these dynamics is a key challenge to understanding multi-electron interactions and resonant processes occurring in any system more complicated than the hydrogen atom [4–7]. However, the accurate characterization of photoionization dynamics requires the phase information acquired by the electron wavepacket during the transition from the ground state to the excited state in the ionization process.

There has been a large amount of interest in characterizing this phase information in the past years via reconstruction of attosecond beating by interference of two-photon transitions (RABBITT) [8, 9] or via a fully optical interferometric technique [10] which requires the use of discrete harmonics of an attosecond pulse train. Such methods lead to a coarse energy sampling and cannot resolve fast oscillations in the group delay as a function of energy. Recently, there has been interest in the analysis of continuous spectrograms from isolated attosecond pulses to increase the energy resolution of the relative phase of the emitted electron wavepackets [2, 3, 11, 12]. However, these methods are still encumbered by many approximations that limit their overall effectiveness.

In this work, we develop a new method for the complete characterization of photoelectron wavepackets using photoelectron streaking spectrograms from isolated attosecond pulses which we call absolute complex

dipole transition matrix element reconstruction (ACDC). The ACDC method is not limited by any approximation other than the strong-field approximation (SFA) used to model the photoionization and streaking process, enabling unprecedented accuracy in the retrieval of the photoelectron wavepacket's phase across a continuous spectrum of electron energies. Applying ACDC to simultaneously measured photoelectron streaking spectrograms from Ar and Ne, we reveal subtle dynamics in the group delay of the photoionization process from Ar that would have been impossible to resolve using prior techniques that sampled the group delay at discrete energy points.

This paper is structured as follows. In section 2 we start with an overview of phase-retrieval techniques and their application in phase and group delay analysis of photoelectron wavepackets. In section 3 we introduce and briefly review the so-called wavepacket approximation [11, 13], that prevents conventional attosecond pulse characterization algorithms from accurately retrieving the complete electron wavepacket from streaking spectrograms. In section 4, we introduce the ACDC method, demonstrating its capability of overcoming the wavepacket approximation to fully characterize electron wavepackets and attosecond time delays in photoemission to within the limits of the SFA. Finally, in section 5, we use the ACDC method to reconstruct the dipole phase of electron wavepackets excited from Ar using experimental streaking measurements.

Our results agree very well with the average group delay measurements using discrete harmonics [10], showing almost a π shift in phase at photon energies ranging from 26 to 30 eV, corresponding to the energy position of the well-known $3s3p^6np$ autoionizing series of Ar [14]. Furthermore, the ACDC reconstruction reveals new group-delay features between 30 and 35 eV that could not be resolved by other techniques. Our results emphasize the importance of the complete and continuous phase retrieval method we use here. We believe that, this work opens the door to more complex studies such as photoelectron excitation dynamics in molecular systems.

2. Extreme-ultraviolet phase retrieval techniques for photoelectron wavepacket analysis

To experimentally investigate attosecond photoemission dynamics, two methods are commonly used: (1) RABBITT [8, 9]; and (2) the photoelectron streaking from single attosecond pulses (SAPs) [15]. Both techniques employ a pump–probe scheme, where an extreme-ultraviolet (XUV) attosecond pump pulse initiates electron dynamics and an infrared (IR) probe pulse interrogates the temporal evolution of the released electrons as the delay τ between pump and probe is varied. While the RABBITT technique uses an attosecond pulse train (APT) in combination with a weak ($<10^{11}$ W cm^{-2}) and typically long IR ($\sim$30 fs) pulse, the photoelectron streaking method uses an SAP and a few-cycle IR ($<$6 fs) as a pump and probe, respectively.

In RABBITT, the spectrum of the applied APT only comprises odd multiples $2q+1$ (q is an integer number) of the fundamental IR frequency ω_{IR} giving rise to a discrete photoelectron spectrum. Due to the presence of the weak IR probe field the ionized photoelectrons may absorb or emit one additional IR photon leading to so-called sidebands in between two consecutive harmonic energies. Due to the discrete nature of the resulting photoelectron spectrum, the retrieved phase is coarsely sampled by twice the fundamental photon energy ($2\hbar\omega_{\mathrm{IR}} \sim 3$eV, where $\hbar$ is the reduced Plank constant). A different and fully optical approach for characterizing electron wavefunctions and to extract photoionization dynamics information is described in [10] where the authors used an XUV–XUV time-resolved interferometry technique that has been recently proposed to extract the dipole phase difference between two atomic species from which the XUV attosecond pulse trains where generated [10]. However, this technique only allows sampling of the accumulated phase of the escaping electrons at energy points that are separated by $2\hbar\omega_{\mathrm{IR}}$, i.e. at energy positions corresponding to the XUV harmonic peaks.

On the other hand, in the streaking measurements the photoelectrons are released upon the absorption of an XUV photon from an SAP in presence of a few-cycle IR pulse, which streaks the liberated electron wavepackets in the continuum to different final momenta. Since different original kinetic energy states are mapped to equivalent final kinetic energy states, there is interference of the electron pathways providing access to the original phase information of the photoemittted electron wavepacket, which can be retrieved with numerical analysis. Since the ionizing SAP contains all energies within its spectral bandwidth, the spectral phase of the electron wavepacket is sampled in a continuous manner, with no fundamental limitation on the energy sampling resolution.

The collected spectral phase of the photoionization and streaking process φ_{stk} can be written as a sum of three main contributing terms [16], i.e.

$$\varphi_{\mathrm{stk}} = \varphi_{\mathrm{XUV}} + \varphi_{\mathrm{W}} + \varphi_{\mathrm{CLC}} \tag{1}$$

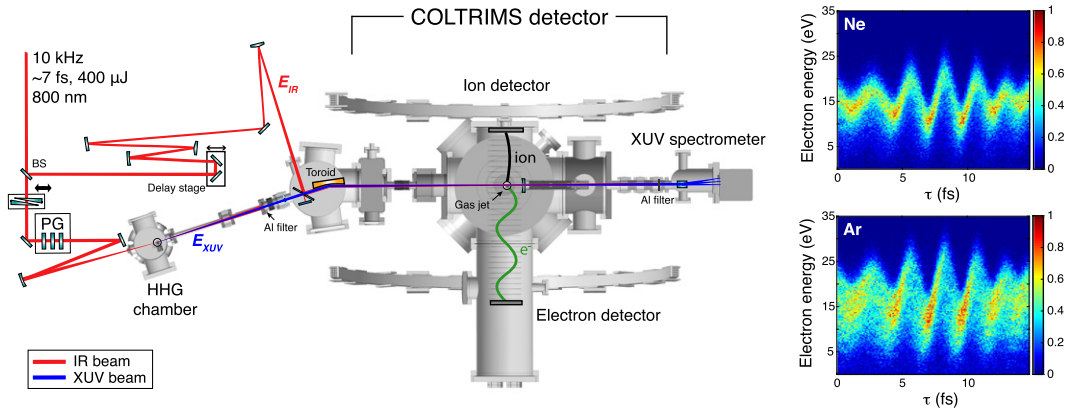

Figure 1. Scheme of the experimental setup including the COLTRIMS detector used to simultaneously measure the streaking spectrograms of Ne (top) and Ar (bottom) considered in this work. The red line represents the path of the IR beam which is spited in two parts by the beam splitter (BS). 80% is used to generate, using the polarization gating (PG) scheme, the XUV pump beam (E_{XUV}) while the remaining 20% is used as the probe streaking field (E_{IR}). The scheme of the experimental setup has been adapted from [19].

where φ_{XUV} is the attochirp phase of the SAP, φ_{W} is the Wigner phase and φ_{CLC} is the Coulomb-laser coupling phase which takes into account the extra phase that the photoemitted electron wavepacket acquires due to the interaction with both the long-range Coulomb potential and the IR streaking field, very similar to the continuum–continuum phase in the RABBITT technique [17].

The derivative of the retrieved spectral phase $\varphi_{\mathrm{stk}}(E)$ corresponds to the group delay (GD) of the excited electron wavepacket, i.e.

$$\mathrm{GD} = \frac{\partial \varphi_{\mathrm{stk}}(E)}{\partial E}. \tag{2}$$

The attochirp contribution to φ_{stk} can be eliminated by computing the GD difference between two different species measured simultaneously and subject to the same ionizing XUV spectrum. This requires the use of a coincidence detection apparatus such as the cold target recoil ion momentum spectrometer (COLTRIMS) [18]. Experimental streaking spectrograms measured simultaneously in Ar and Ne using the COLTRIMS apparatus [19] and which will be object of our analysis in section 5 of this work are shown in figure 1.

The measurement-induced contribution φ_{CLC} can be extracted from numerical calculation [20] such that by comparison of two simultaneously measured streaking spectrograms the extracted phase has only the Wigner contribution. However, as alluded to earlier, access to $\varphi_{\mathrm{W}}(E)$ from photoelectron streaking measurements requires a numerical retrieval algorithm.

Frequency resolved optical gating for complete retrieval of attosecond bursts (FROG-CRAB) [21, 22] is a well-established and widely used method for characterizing the time-domain profile of XUV pulses (both amplitude and phase) from streaking spectrograms. A critical analysis in retrieving the phase of the photoemitted electron wavepacket using FROG-CRAB methods has been carried out by Wei *et al* [1] where they point out limitations of the method, namely the central momentum approximation and what they call the wavepacket approximation (WPA) [11, 13]. In their work, they were unable to overcome these limitations to fully recover the phase of the photoelectron wavepacket. While others have shown the ability to circumvent the central-momentum approximation [23], to our knowledge the wavepacket approximation remains the limiting factor in accurate photoelectron retrieval. In the following sections, we define the wavepacket approximation and demonstrate why it is so problematic. We then present the ACDC method which overcomes the wavepacket approximation and use it with the experimental data shown in figure 1 to reveal newly observed group-delay dynamics in photoemission from Ar.

3. Wavepacket approximation (WPA)

The complex amplitude of a photoelectron going from the ground state to the final state with momentum k can be expressed within the SFA

$$\tilde{a}_{\mathrm{SFA}}(k,\tau) = -\mathrm{i}\int_{-\infty}^{+\infty} \mathrm{d}t \tilde{d}\left(k + A\left(t\right)\right) \tilde{E}_{\mathrm{XUV}}(t-\tau)\mathrm{e}^{\mathrm{i}\phi(k,t)}\mathrm{e}^{\mathrm{i}\left(I_p + \frac{k^2}{2}\right)t}, \tag{3}$$

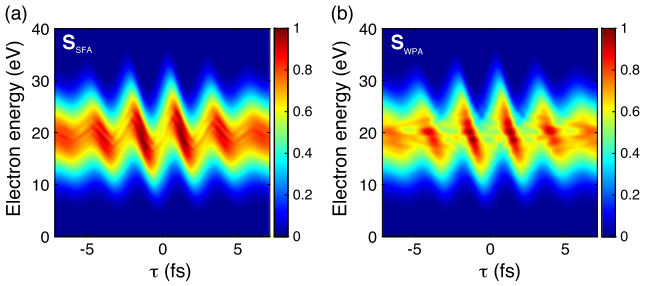

Figure 2. Simulated streaking spectrograms using (a) the SFA model $S_{\mathrm{SFA}}(k,\tau) = |\tilde{a}_{\mathrm{SFA}}(k,\tau)|^2$ and (b) using the WPA, i.e. $S_{\mathrm{WPA}}(k,\tau) = |\tilde{a}_{\mathrm{WPA}}(k,\tau)|^2$. We observe a percentage difference between the two spectrograms shown here of up to 35% mainly concentrated around the central energy of the spectrogram.

where $\tilde{d}(k)$ is the dipole transition matrix element (DTME), τ the time delay between the XUV pump pulse and the IR probe pulse, $\tilde{E}_{\mathrm{XUV}}(t)$ is the XUV field in time domain and $A(t)$ the vector potential of the IR electric field from which it can be calculated, $E_{\mathrm{IR}}(t) = -\frac{\partial}{\partial t}A(t)$.

The phase modulation term, $\phi(k,t)$, resulting from the accumulated phase of the electron during the streaking process reads

$$\phi(k,t) = -\int_{t}^{+\infty} \mathrm{d}t' \left[kA\left(t'\right) + \frac{1}{2}A^2(t')\right]. \tag{4}$$

The measured photoelectron spectrum is given by the probability of measuring an electron with momentum k and delay τ, i.e. $S_{\mathrm{SFA}}(k,\tau) = |\tilde{a}_{\mathrm{SFA}}(k,\tau)|^2$.

In absence of the IR electric field, the XUV pulse, ionizing the target gas, generate a photoelectron wavepacket that can be expressed in the energy domain as

$$\tilde{\chi}(E) = \tilde{E}_{\mathrm{XUV}}\left(I_P + \frac{k^2}{2}\right)\tilde{d}(E). \tag{5}$$

Introducing the expression of the wavepacket (5) into equation (3) we can rewrite the SFA complex amplitude within the WPA as follows

$$\tilde{a}_{\mathrm{WPA}}(k,\tau) = -\mathrm{i}\int_{-\infty}^{+\infty} \mathrm{d}t\tilde{\chi}(t-\tau)\,\mathrm{e}^{\mathrm{i}\phi(k,t)}\mathrm{e}^{\mathrm{i}\left(I_P+\frac{k^2}{2}\right)t}. \tag{6}$$

As explained in [11], the WPA is not an exact theory but rather an approximation to the SFA model given by equation (3), which is considered the model better describing the physics of the streaking process. The difference between the spectrogram $S_{\mathrm{SFA}}(k,\tau)$ and $S_{\mathrm{WPA}}(k,\tau) = |\tilde{a}_{\mathrm{WPA}}(k,\tau)|^2$ can be seen by comparing S_{SFA} and S_{WPA} as we show in figure 2.

Most photoelectron retrieval methods based on FROG-CRAB, when used to characterize the electron wavepacket $\tilde{\chi}(E)$, rely on the WPA (i.e. they use $\tilde{a}_{\mathrm{WPA}}$ to model the streaking process rather than $\tilde{a}_{\mathrm{SFA}}$), which leads to significant errors in the retrieved phase response and group delay as the physics of the experiment is better described by $\tilde{a}_{\mathrm{SFA}}$ [see appendix A for further analysis (http://stacks.iop.org/NJP/22/053028/mmedia)]. In the following sections, we introduce the ACDC method which overcomes the WPA, enabling a complete characterization of the photoemitted electron wavepacket.

4. Absolute complex DTME reconstruction (ACDC) algorithm

In this section we describe the method of the ACDC algorithm to retrieve the DTME ($\tilde{d}$), when both the XUV and IR pulses are known quantities.

Starting from the SFA expression of the complex amplitude of the photoemitted electron wavepacket given by equation (3), we now approximate $\tilde{d}$ using the first order Taylor expansion at such that

$$\tilde{d}\left(k + A(t+\tau)\right) \approx \tilde{d}\left(k\right) + \tilde{d}'(k)A(t+\tau), \tag{7}$$

where $\tilde{d}'(k) = \partial_k\tilde{d}$. In this way we can rewrite the complex amplitude describing the transition from the ground state to the final momentum k as:

$$\tilde{a}_{\mathrm{SFA}}(k,\tau) \approx \tilde{d}\left(k\right)\tilde{\Gamma}(k,\tau) + \tilde{d}'(k)\tilde{\beta}(k,\tau) \tag{8}$$

where we introduced

$$\tilde{\Gamma}(k,\tau) = -\mathrm{i}\int_{-\infty}^{+\infty} \mathrm{d}t \tilde{E}_{\mathrm{X}}(t) \mathrm{e}^{\mathrm{i}\phi(k,t+\tau)} \mathrm{e}^{\mathrm{i}\left(I_p t + \frac{k^2 t}{2}\right)} \tag{9}$$

and

$$\tilde{\beta}(k,\tau) = -\mathrm{i}\int_{-\infty}^{+\infty} \mathrm{d}t A(t+\tau)\, \tilde{E}_{\mathrm{X}}(t)\, \mathrm{e}^{\mathrm{i}\phi(k,t+\tau)} \mathrm{e}^{\mathrm{i}\left(I_p t + \frac{k^2 t}{2}\right)}. \tag{10}$$

When we numerically sample the momentum and time delay components, we approximate the derivative of $\tilde{d}$ as:

$$\tilde{d}'[m] = \frac{\tilde{d}[m+1] - d[m-1]}{\Delta k[m]} \tag{11}$$

where m is the sample number in energy and $\Delta k[m] = k[m+1] - k[m-1]$. Using this we can write

$$\tilde{a}_{\mathrm{SFA}}[l,m] = \tilde{d}[m]\,\tilde{\Gamma}[l,m] + \frac{\tilde{d}[m+1]\,\tilde{\beta}[l,m]}{\Delta k[m]} - \frac{\tilde{d}[m-1]\,\tilde{\beta}[l,m]}{\Delta k[m]} \tag{12}$$

where l is the sample number of time delays.

Using the same minimization strategy as Volkov transform generalized projections algorithm (VTGPA) [23] we define the matrix $\tilde{a}'[l,m]$ as

$$\tilde{a}'[l,m] = \sqrt{P[l,m]}\mathrm{e}^{\mathrm{i}\arg(\tilde{a}_{\mathrm{SFA}}[l,m])} \tag{13}$$

that is the measured spectrogram amplitude $P[l,m]$ projected onto the computed spectrogram $\tilde{a}_{\mathrm{SFA}}[l,m]$. From this we can define the figure of merit M

$$M = \sum_l \sum_m \left(\tilde{a}_{\mathrm{SFA}}[l,m] - \tilde{a}'[l,m]\right) \times c \cdot c \tag{14}$$

and the value of $\tilde{d}[m] = d[m]\mathrm{e}^{\mathrm{i}\phi[m]}$ that minimizes M by solving the system of equations

$$\frac{\partial M}{\partial d[m]} = 0; \quad \frac{\partial M}{\partial \phi[m]} = 0. \tag{15}$$

In appendix B we report the full derivation of the expression of $\tilde{d}$.

For low streaking intensities ($\leqslant 1 \times 10^{10}$ W cm^{-2}), this approach accurately reconstructs $\tilde{d}$ (see simulation results in appendix B). However, when the streaking intensity, and thus the streaking vector potential, is large ($>1 \times 10^{10}$ W cm^{-2}), the Taylor expansion used in equation (7) becomes inadequate. Expanding to higher orders was found to be overly cumbersome, and in the end the most effective approach in this case was to: (1) use the analytical method described above using the first order Taylor expansion as a first step to estimate the amplitude and phase of $\tilde{d}$; and (2) apply a numerical stochastic gradient descent algorithm to refine the estimated DTME from (1), bringing it much closer to the actual solution.

For step (2), we used a stochastic gradient descent algorithm along with Adam (adaptive momentum estimation) optimizer [24]. The use of step (1) is justified by the fact that, the convergence to local minima of the cost function, when using the step (2), results faster.

For simplicity, we leave the technical description, together with the effect of the approximation of the first order Taylor expansion, in appendix B. Additionally, in appendix C we show the robustness of the ACDC method on simulated spectrograms using different streaking parameters, i.e. IR intensity, XUV bandwidth and XUV chirp.

In figure 3, we show the result of the ACDC method when reconstructing a simulated spectrogram from Ar. Artificial Poisson noise was added to the simulated spectrogram to mimic the noise observed in the experimental data (figure 1).

Since we want to reconstruct the DTME from experimental spectrograms, we also considered parameters of both the XUV and the IR field similar to the experimental conditions that we will consider in the next section. In particular, we used an IR intensity of 3×10^{12} W cm^{-2} while the XUV spectrum (grey shaded area in figure 3) resembles the actual spectrum used during experiments. The red line in figure 3 represents the reconstructed GD using the ACDC method in absence of noise while the green curve shows the result in presence of noise level comparable to the experiment (see appendix D for details of noise analysis).

Despite the fact that fluctuations due to noise are still present, we observe a good agreement with the theoretical curve used as the input for the GD$^{\mathrm{Ar}}$ (black line) [3] over the entire energy window considered for the reconstruction, including the rapid group delay fluctuations from 34–38 eV. This result validates the algorithm's robustness against noise and its applicability to experimental measurements which is considered in the next section.

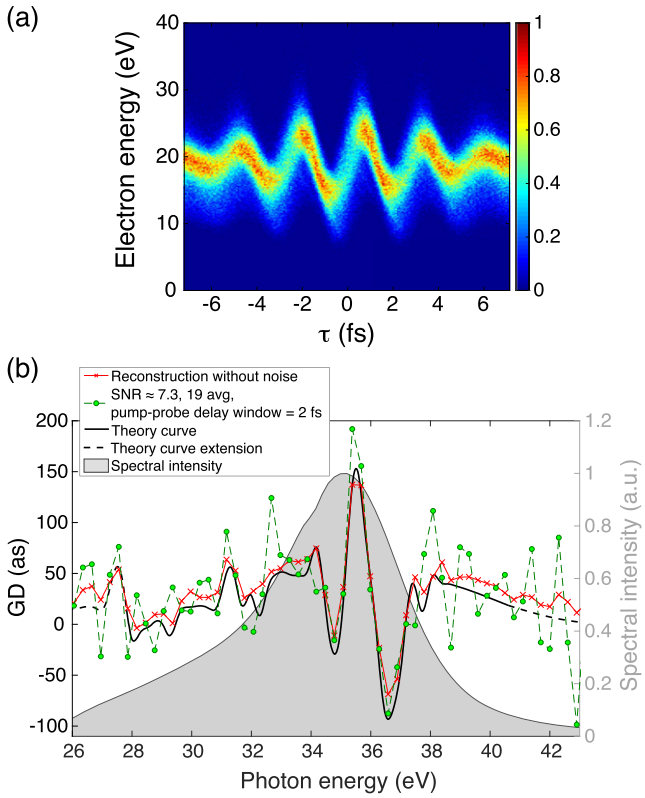

Figure 3. (a) Simulated streaking spectrogram with a Poisson noise level comparable to the experimental conditions. (b) Retrieved GD with ACDC without noise (red line) and in presence of noise (green line). The green line is the weighted average of 19 reconstructions on different pump probe delay windows of 2 fs. The theory curve (black line) used as input to generate the simulated spectrogram shown in (a) is from reference [3]. In order to be able to simulate the spectrograms avoiding unphysical abrupt jumps in the simulated spectrogram amplitude, we extended the theoretical curve below 27.8 eV and above 40.5 eV (black dashed lines). The grey shaded area shows the XUV spectral intensity reproducing the experimental case.

5. Experimental reconstruction of the Ar dipole phase

In this section we retrieved the dipole phase of Ar from the experimental spectrogram shown in figure 1 using ACDC. In figure 4 the blue line and blue shaded area show the reconstructed Ar dipole phase resulting from 36 averages using the ACDC algorithm and its standard deviation, respectively. For the interested reader, the details of the reconstruction procedure can be found in appendix E.

The dipole phase difference between Ne and Ar have also been measured experimentally by Azoury *et al* using optical attosecond interferometry [10]. Adapting their result by flipping the sign and adding the Ne dipole phase from reference [25] (yellow squares in figure 4), we observe an excellent agreement with the ACDC reconstruction over the full energy spectrum. However, since the ACDC algorithm resolves the phase in a continuous manner, a much finer phase structure is resolved as a function of photon energy.

In the present measurement we sampled the Ar DTME every 0.15 eV, while in [10] it was every ∼3.1 eV due to the spacing of the discrete XUV harmonics.

The ACDC result reveals a pronounced peak in the dipole phase of Ar between 30 to 32 eV [label (b) in figure 4] and a subsequent dip in the energy region from 33 to 35 eV [label (c) in figure 4] which cannot be described by a piecewise linear fit between the data points from [10].

In order to compare the obtained GD^{Ar} with the differential group delay ΔGD^{ArNe} reported from other experiments, we subtracted the GD of Ne from GD^{Ar} using the theoretical calculation from reference [25]. The result is shown in figure 5 by the blue curve together with the blue shaded region, which represents the standard deviation. We note the persistent rapid variations of the ΔGD^{ArNe} that lie in the energy region where the Ar autoionizing states are located as displayed by the black vertical lines. While these oscillations are intriguing, they are near the noise limits of the retrievals from our current measurement data, and to fully confirm that those oscillations are signature of the $3s3p^6np$ autoionizing states will require further investigations that go beyond the scope of this work.

In figure 5 we also plot several data points from previously reported RABBITT-like measurements of the average group delay ΔGD^{ArNe} (green, blue and grey squares [2], magenta circles [26], and yellow

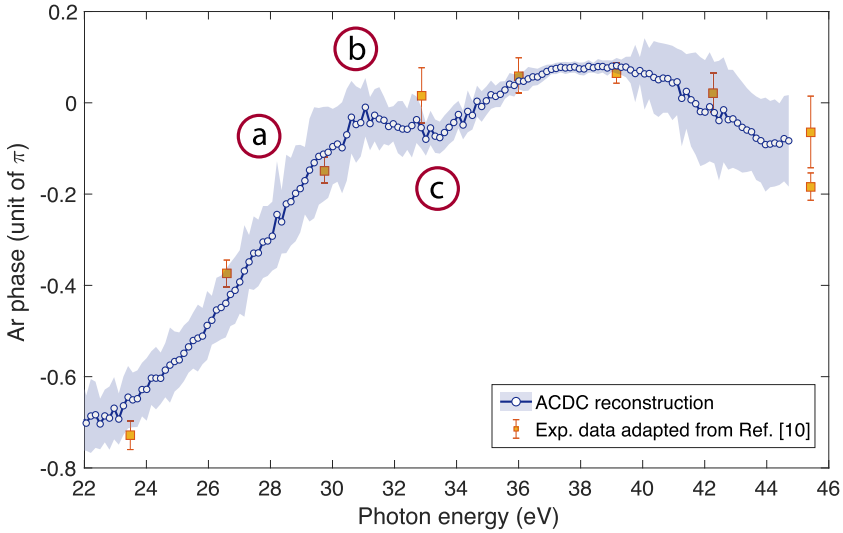

Figure 4. The blue curve displays the average of 36 retrieved Ar dipole phases from the reconstruction of experimental measurement using the ACDC algorithm. The yellow symbols are adapted experimental result from reference [10] and shifted to within a constant offset. The labels (a)–(c) refer to the discussion in the main text.

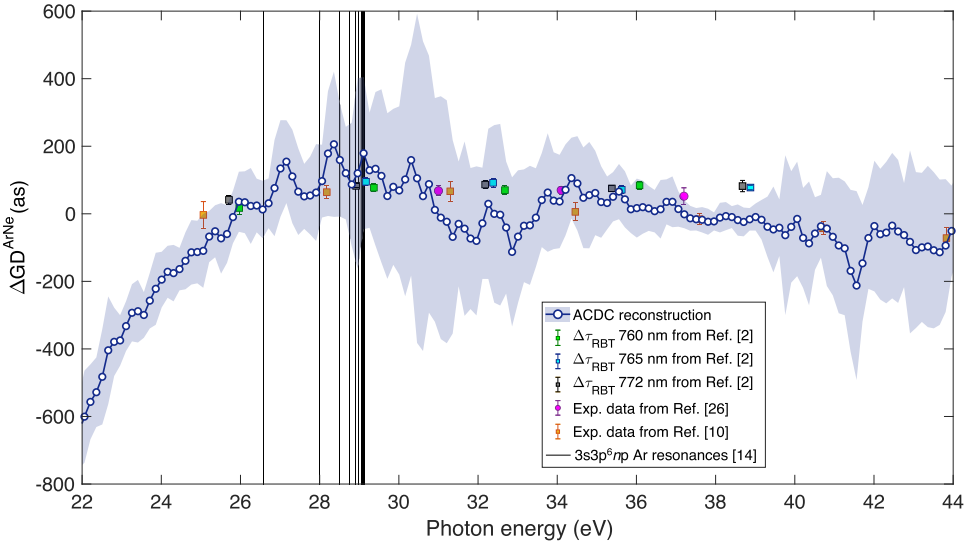

Figure 5. Retrieved ΔGD^{ArNe} from experimental streaking measurement using the ACDC algorithm averaging 36 reconstructions is shown by the blue curve together with its standard deviation (blue shaded area). RABBITT measurements from reference [2] (green, blue and grey squares) and from reference [26] (magenta circles) are displayed. Results from a fully optical interferometric technique from reference [10] are also plotted with yellow squares. The black vertical lines show the calculated $3s3p^6np$ autoionizing series of Ar from reference [14].

squares [10]). We observe that, between 28 to 30 eV the ACDC result retrieves, on average, a higher ΔGD^{ArNe} compared to RABBITT measurements while, between 30 to 34 eV, the ACDC result predicts a lower value. These correspond to the regions labelled as (a)–(c) in figure 4. This discrepancy between ΔGD^{ArNe} retrieved by ACDC and the RABBITT measurements arises due to the ACDC's ability to more finely sample the phase of the DTME. Indeed, the comparison between the ΔGD^{ArNe} curve reconstructed with the ACDC from the SAP streaking measurement and the other data points derived from discrete energy measurements using the RABBITT-like techniques will never perfectly overlap wherever the phase is not well-fit by a piecewise linear phase function between the RABBITT sampling points. For example, after downsampling the reconstructed phase of Ar using the ACDC algorithm from figure 4 at the energy points separated by ∼3.1 eV of the experimental work presented in reference [10] (yellow squares) and then computing the ΔGD^{ArNe}, we obtain the green diamonds shown in figure 6 which overlap almost perfectly with the datapoints from reference [10] (yellow squares).

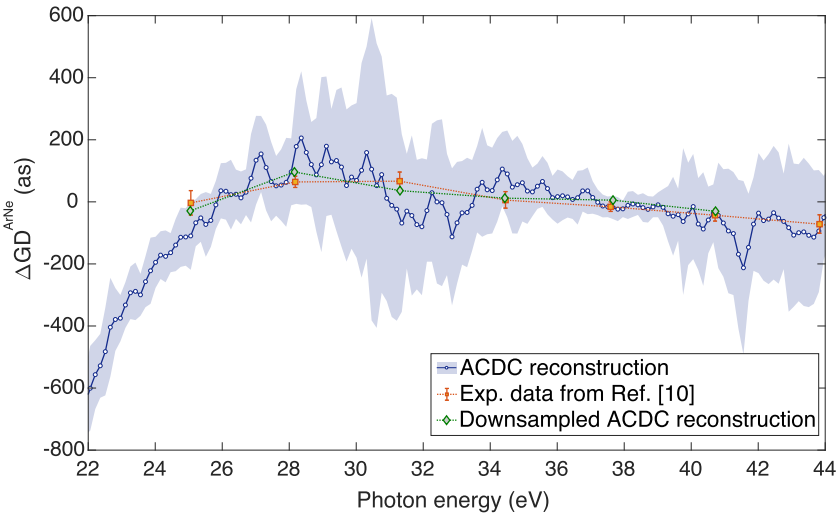

Figure 6. The green diamonds show the retrieved ΔGD^{ArNe} computed from the reconstructed dipole phase of Ar using the ACDC algorithm (blue curve in figure 4) downsampled at the energy points separated by ∼3.1 eV of the experimental result presented in reference [10] (yellow squares).

6. Conclusion

In this work, we have addressed long-standing issues in the characterization of electron wavepackets using streaking spectrograms. We demonstrated that the WPA hinders the accurate retrieval of an electron wavepacket when using conventional attosecond pulse characterization algorithms. To overcome this approximation and to exploit the continuous energy resolution of the photoelectron streaking technique, we introduced a new method for electron wavepacket characterization: ACDC. This algorithm has the ability to extract the electron wavepacket phase, thus the photoemission GD, within the limitations only imposed by the SFA, using well-established attosecond streaking methods.

We used the new algorithm to reconstruct the absolute GD of Ar from experimental measurements. The result highlights the importance of reconstructing the dipole phase in a continuous manner in order to resolve variations in the GD as a function of energy which would not be resolved by RABBITT-like techniques. Interestingly, the ACDC reconstruction reveals features in the ΔGD^{ArNe} in the energy region corresponding to that of the $3s3p^6np$ autoionizing series of Ar however a deeper investigation of this energy region is required using additional measurements and theoretical modelling.

We believe that with the ACDC algorithm, we can now fully exploit the potential offered by photoelectron streaking using SAPs. Specifically, we can now access the complete and continuous electron wavepacket phase profile of an unknown target assuming that the DTME of one target gas species is known, allowing the direct measurement of electron dynamics in more complicated systems, such as molecules. Experimental effort in this direction is currently underway.

Acknowledgments

This work was supported by NCCR Molecular Ultrafast Science and Technology (NCCR MUST), research instrument of the Swiss National Science Foundation (SNSF).

P Keathley acknowledges support by the Air Force Office of Scientific Research (AFOSR) Grant under Contract No. FA9550-19-1-0065.

ORCID iDs

P D Keathley https://orcid.org/0000-0003-1325-1768

References

[1] Wei H, Morishita T and Lin C D 2016 Critical evaluation of attosecond time delays retrieved from photoelectron streaking measurements *Phys. Rev.* A **93** 1–14

[2] Cattaneo L, Vos J, Lucchini M, Gallmann L, Cirelli C and Keller U 2016 Comparison of attosecond streaking and RABBITT *Opt. Express* **24** 29060
[3] Sabbar M *et al* 2017 Erratum: resonance effects in photoemission time delays *Phys. Rev. Lett.* **119** 4–5
[4] Kotur M *et al* 2016 Spectral phase measurement of a Fano resonance using tunable attosecond pulses *Nat. Commun.* **7** 1–6
[5] Gruson V *et al* 2016 Attosecond dynamics through a Fano resonance: monitoring the birth of a photoelectron *Science* **354** 734–8
[6] Kaldun A *et al* 2017 Observing the ultrafast buildup of a Fano resonance in the time domain *2017 Conf. Lasers Electro-Optics, CLEO 2017 - Proc.* vol 2017 pp 1–2
[7] Cirelli C *et al* 2018 Anisotropic photoemission time delays close to a Fano resonance *Nat. Commun.* **9** 955
[8] Paul P M *et al* 2001 Observation of a train of attosecond pulses from high harmonic generation *Science* **292** 1689–92
[9] Muller H G 2002 Reconstruction of attosecond harmonic beating by interference of two-photon transitions *Appl. Phys.* B **74** 17–21
[10] Azoury D *et al* 2019 Electronic wavefunctions probed by all-optical attosecond interferometry *Nat. Photon.* **13** 54–9
[11] Zhao X, Wei H, Wei C and Lin C D 2017 A new method for accurate retrieval of atomic dipole phase or photoionization group delay in attosecond photoelectron streaking experiments *J. Opt.* **19** 114009
[12] Sabbar M *et al* 2015 Resonance effects in photoemission time delays *Phys. Rev. Lett.* **115** 1–5
[13] Yakovlev V S, Gagnon J, Karpowicz N and Krausz F 2010 Attosecond streaking enables the measurement of quantum phase *Phys. Rev. Lett.* **105** 3–6
[14] Carette T, Dahlström J M, Argenti L and Lindroth E 2013 Multiconfigurational Hartree-Fock close-coupling ansatz: application to the argon photoionization cross section and delays *Phys. Rev.* A **87** 1–13
[15] Itatani J, Quéré F, Yudin G L, Ivanov M Y, Krausz F and Corkum P B 2002 Attosecond streak camera *Phys. Rev. Lett.* **88** 4
[16] Dahlström J M *et al* 2013 Theory of attosecond delays in laser-assisted photoionization *Chem. Phys.* **414** 53–64
[17] Dahlström J M, L'Huillier A and Maquet A 2012 Introduction to attosecond delays in photoionization *J. Phys. B: At. Mol. Opt. Phys.* **45** 183001
[18] Dörner R *et al* 2000 Cold target recoil ion momentum spectroscopy: a 'momentum microscope' to view atomic collision dynamics *Phys. Rep.* **330** 95–192
[19] Sabbar M *et al* 2014 Combining attosecond XUV pulses with coincidence spectroscopy *Rev. Sci. Instrum.* **85** 103113
[20] Pazourek R, Nagele S and Burgdörfer J 2013 Time-resolved photoemission on the attosecond scale: opportunities and challenges *Faraday Discuss.* **163** 353–76
[21] Mairesse Y and Quéré F 2005 Frequency-resolved optical gating for complete reconstruction of attosecond bursts *Phys. Rev.* A **71** 1–4
[22] Gagnon J, Goulielmakis E and Yakovlev V S 2008 The accurate FROG characterization of attosecond pulses from streaking measurements *Appl. Phys.* B **92** 25–32
[23] Keathley P D, Bhardwaj S, Moses J, Laurent G and Kärtner F X 2016 Volkov transform generalized projection algorithm for attosecond pulse characterization *New J. Phys.* **18** 1–14
[24] Kingma D P and Ba J 2014 Adam: a method for stochastic optimization arXiv:1412.6980v9
[25] Bhardwaj S, Son S K, Hong K H, Lai C J, Kärtner F X and Santra R 2013 Recombination-amplitude calculations of noble gases, in both length and acceleration forms, beyond the strong-field approximation *Phys. Rev.* A **88** 1–7
[26] Guénot D *et al* 2014 Measurements of relative photoemission time delays in noble gas atoms *J. Phys. B: At. Mol. Opt. Phys.* **47** 245602